Tailoring NIR-II photoluminescence of single thiolated Au_{25} nanoclusters by selective binding to proteins

Franck Bertorelle,[a],[b] K. David Wegner,[c] Martina Perić Bakulić,[d] Hussein Fakhouri, [a],[d] Clothilde Comby-Zerbino,[a] Amin Sagar,[e] Pau Bernadó,[e] Ute Resch-Genger,[c] Vlasta Bonačić-Koutecký,[d], [f] Xavier Le Guével[g],* and Rodolphe Antoine[a],*

[a] Dr. Franck Bertorelle, Hussein Fakhouri, Clothilde Comby-Zerbino and Dr. Rodolphe Antoine
Institut lumière matière, UMR5306, Université Claude Bernard Lyon1-CNRS, Univ. Lyon 69622, Villeurbanne cedex, France.
rodolphe.antoine@univ-lyon1.fr

[b] Dr. Franck Bertorelle
Nantes Université, CNRS, US2B, UMR 6286, F-44000 Nantes, France

[c] Dr. K. David Wegner and Prof. Ute Resch-Genger
Federal Institute for Materials Research and Testing (BAM), Richard-Willstaetter-Str. 11, 12489 Berlin, Germany

[d] Martina Perić Bakulić, Hussein Fakhouri and Prof. Vlasta Bonačić-Koutecký
Center of Excellence for Science and Technology-Integration of Mediterranean Region (STIM) at Interdisciplinary Center for Advanced Sciences and Technology (ICAST), University of Split, Poljička cesta 35, 21000 Split, Croatia

[e] Dr. Amin Sagar and Dr. Pau Bernadó
Centre de Biologie Structurale, Université de Montpellier, INSERM, CNRS. 29 rue de Navacelles 34090 Montpellier – France

[f] Prof. Vlasta Bonačić-Koutecký
Chemistry Department, Humboldt University of Berlin, Brook-Taylor-Strasse 2, 12489 Berlin, Germany

[g] Dr. Xavier Le Guével
Institute for Advanced Biosciences, Univ. Grenoble Alpes/INSERM1209/CNRS-UMR5309, Grenoble, France. xavier.le-guevel@univ-grenoble-alpes.fr

Supporting information for this article is given via a link at the end of the document.

Abstract: Atomically precise gold nanoclusters are a fascinating class of nanomaterials that exhibit molecule-like properties and have outstanding photoluminescence. Their ultrasmall size, molecular chemistry, and biocompatibility make them extremely appealing for selective biomolecule labeling in investigations of biological mechanisms at the cellular and anatomical levels. In this work, we report a simple route to incorporating a preformed Au_{25} nanocluster into a model bovine serum albumin (BSA) protein. A new approach combining small-angle X-ray scattering and molecular modeling provides a clear localization of a single Au_{25} within the protein to a cysteine residue on the gold nanocluster surface. Attaching Au_{25} to BSA strikingly modifies the PL properties with enhancement and a redshift in the second near-infrared window (NIR-II). This study paves the way to controlling the design of selectively sensitive probes in biomolecules through a ligand-based strategy to enable the optical detection of biomolecules in a cellular environment by live imaging.

Introduction

Gold nanoclusters (Au NCs) are at the forefront of nanomaterials that can be used for bio-applications due to their high colloidal stability, ultra-small size, low toxicity, high biocompatibility, and size-tunable photoluminescence (PL).[1] The ability to tailor their surface offers great advantages to label (bio)molecules of interest and monitor them using advanced imaging techniques.[2] However, Au NCs possess intrinsically quite low quantum yields (QYs); thus, several rational strategies have been developed to tailor and increase their PL properties.[3] For example, one strategy involves increasing the organic shell rigidity, which protects the metal core and has led to several-fold PL enhancement in the near-infrared NIR-I (700-900 nm)[4] and NIR-II (900-1700 nm)[5] regions. This PL increase has been associated with the reduction of water molecules in the proximity of the Au NC surface, which minimizes non-radiative recombination processes.[6] A second strategy relies on the fine tuning of the surface chemistry.[7] Millstone's team conducted an extensive study demonstrating the influence of thiolated ligands[8] on the near infrared emission of ultrasmall metal (gold, silver, copper) nanoparticles.[9] In addition, it was shown that the addition of a thiolated ligand is important, and the denticity of the ligand used can influence the PL band and QY. For example, adding a short dithiol co-ligand to the Au NC surface led to a 6-fold increase in the QY with PL enhancement in the 1100-1300 nm range,[10] which allowed the researchers to monitor them noninvasively in vivo down to a 4 mm depth in mice.[11]

Protecting Au NCs within large biomolecules such as proteins can be a rational and elegant strategy for engineering the PL of Au NCs and lead to ideal platforms for biomedical applications.[12] The presence of intrinsic reducing agents and sulfur-containing chemical groups in proteins enables the one-step protection of metal NCs. The synthesis of fluorescent protein-directed Au NCs using albumin (BSA, bovine serum albumin) as both a reductant and stabilizer was pioneered by Xie et al.[13] Following this seminal work, various NCs were synthesized with different proteins, showing very high PL brightness and good photostability for biolabeling/imaging purposes.[14] Although some studies have shown that proteins retain their structure and biological activity upon protein-directed NC formation,[15] there is an increasing number of

studies demonstrating that the global (and local) structure of proteins is altered after NC formation; these studies were often performed under quite harsh conditions (pH 12, for example), which can also affect the structure of the proteins.[16]

Additionally, the exact number of metal atoms in protein-directed NCs and their localization within the protein are still under debate, preventing the development of a clear structure-property relationship.[3a] It has been recently shown that clusters in proteins may in fact be composed of sub-units of 8 to 10 atoms located in different parts of the protein, and these sub-units can induce partial denaturation.[17] Clearly, with such alteration of the native state of the protein host and/or uncontrolled formation and location of clusters within proteins, such nanoclusters may present reduced bioactivity and/or biocompatibility, limiting the widespread use of such materials in biomedical research. Therefore, new synthetic methods preserving the structure and bioactivity of incorporated NCs are in high demand. Ligand exchange plays an important role in thiolated nanoclusters, as the flexibility of the gold–sulfur interface enables post-synthetic modification.[18] Additionally, functionalization of gold through ligand exchange has been recently exploited for protein carbonylation detection.[19] As mentioned before, variations in the nature of ligands and the simplicity of the ligand exchange offer great potential to amplify specific properties of the clusters, such as the PL properties.[3a]

In this work, we report the incorporation of a single preformed Au_{25} nanocluster ($Au_{25}(pMBA)_{18}$, pMBA - 4-mercaptobenzoic acid) into bovine serum albumin (BSA) protein selectively anchored to one cysteine residue without drastic modification of the protein structure. The attachment of a single thiolated Au_{25} nanocluster to the protein had a significant effect on its NIR-II emission band with a ~5-fold enhancement of the PL QY. Such water-soluble Au25 NCs attached to BSA display bright infrared emission between 700 nm and 1300 nm, in contrast to previously reported fluorescent BSA-directed Au NCs that only emit in red. Mass spectrometry analysis revealed that Au_{25} NCs is attached to BSA. Small-angle X-ray scattering (SAXS) provided the localization of a Au_{25} NC on the protein via a free cysteine residue, Cys_{34}. To better understand the PL properties of Au_{25} nanoclusters attached to BSA, we synthesized mixed liganded nanoclusters, $Au_{25}pMBA_{(18-x)}Cys_x$ with x=2, 5, 18, through ligand exchange. The origin of NIR-II emission in nanoclusters with mixed ligands determined by optical measurements and density functional theory reveals the key role of the metallic-ligand interface in photophysical pathways.

Results and Discussion

Formation of $Au_{25}pMBA_{18}$ nanoclusters and their attachment to BSA. Au_{25} clusters protected by 18 mercaptobenzoic acid (para isomer) ligands were synthesized as described in a previous study.[20][21] The best results were obtained when a slight excess of $Au_{25}pMBA_{18}$ over BSA (ratio 1.2:1) was used, but the synthesis was also performed with an excess of protein (ratio 1:3). Upon gentle and continuous stirring for 3 days, the Au_{25} nanocluster was incorporated into the BSA protein. A schematic representation of the proposed reaction mechanism is shown in Figure S1. These formed Au_{25}-BSA conjugates were purified using 10% acrylamide SDS–PAGE gel separation. The gel resulted in two bands, which were attributed to $Au_{25}pMBA_{18}$ and Au_{25}-BSA, in contrast with the single band observed for the BSA control (Fig. S2). The slight difference in the positions of the BSA and Au_{25}-BSA bands in the gel indicates that both the charge and overall shape of the protein subtly changed due to the incorporation of the preformed Au_{25} NCs into the BSA protein. We noticed that $Au_{25}pMBA_{18}$ could not bind to BSA even when we used an excess of protein (Fig. S2b). This result could suggest that $Au_{25}pMBA_{18}$ is not stuck to the surface but fixed inside the protein and cannot react anymore.

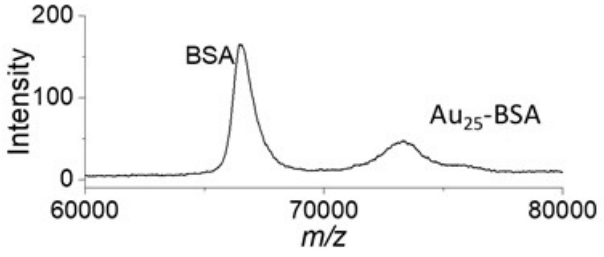


Figure 1: MALDI-TOF spectrum of Au_{25} nanoclusters attached to BSA protein (positive mode).

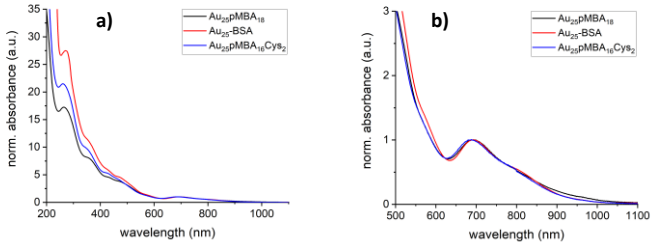


Figure 2: a) Absorption spectra of Au25pMBA18, Au25pMBA16Cys2 and Au25-BSA NCs dispersed in water. b) zoom in 500-1100 nm of absorption spectra. Data normalized on 690 nm absorbance value.

Characterization of Au_{25}-BSA conjugates. Matrix-assisted laser desorption/ionization time-of-flight mass spectrometry (MALDI-TOF MS) was used to characterize the Au_{25}-BSA NCs (Figure 1). In addition to the signature peak of the BSA protein at ~66 kDa, the MALDI spectrum shows an additional peak at higher molecular weight. The molecular weight difference of this peak from BSA was 7.3 kDa, which indicates the attachment of only one gold nanocluster to the

protein, as the mass for one $Au_{25}pMBA_{18}$ nanocluster is 7.68 kDa. Of note is that additional nano-electrospray ionization MS investigations were conducted on BSA and Au_{25}-BSA NCs (see Figure S3). A molecular weight difference of the Au_{25}-BSA NC's peak from BSA was 7.22 kDa confirming MALDI-MS measurements and thus the attachment of only one gold nanocluster to the protein. However, the observed mass shift of the Au_{25}-BSA was lower than expected. This mass shift may be explained by the removal of 2-3 pMBA surface ligands during incorporation into BSA and the replacement of intrinsically available sulfur groups from the cysteine residues in the BSA (see Fig. S4). As shown below, to reveal the key role of the metallic-ligand interface in the photophysical pathways of Au_{25}-BSA NCs, we were able to produce $Au_{25}pMBA_{16}Cys_2$ NCs by ligand exchange (between pMBA and cysteine) from the $Au_{25}pMBA_{18}$ precursor nanocluster. Figure 2 shows the absorption spectra of $Au_{25}pMBA_{18}$, $Au_{25}pMBA_{16}Cys_2$ and Au_{25}-BSA NCs dispersed in water. Both clusters present very similar optical spectra with a band at 690 nm, as well as a broad shoulder at ~800 nm. The absorption spectra of $Au_{25}pMBA_{18}$, Au_{25}-BSA clusters and $Au_{25}pMBA_{16}Cys_2$ are similar to the 25-Au-atom cluster ($Au_{25}(SCH_2CH_2Ph)_{18}$) with a known crystallographic structure (sphere-like shape).[22] Usually, structures cannot be determined from the absorption spectrum alone. However, in this size regime (e.g. 20-25 gold atoms), optical absorption spectra are very different for different cluster sizes.[23] The observed mass shift (7.2-7.3 kDa vs 7.68 kDa) could be explained by the removal of one of two gold atoms during the incorporation of gold nanocluster into BSA. However, just one or two different gold atoms in the gold nanoclusters, e.g. Au_{24}[24] and Au_{23}[25] will lead to different UV-vis spectra (in particular for the red band at 690 nm and the broad shoulder at ~800 nm), which is not the case for larger cluster (e.g. Au_{48} and Au_{46}).[26] For Au_{25} nanoclusters, other aspects may affect the structure-optical relationship, e.g. charge of gold kernel, temperature dependent splitting of molecular orbitals due to spin-orbit interaction, ligand exchange and structural isomerization.[22a] It should be noted that the 800 nm optical absorption shoulder is one of the important absorption feature of $Au_{25}(SR)_{18}$ with −1 charge state.[22a, 27] The fact that such shoulder at 800 nm is observed for the three nanoclusters in Fig. 2 is indicative that this charge state is preserved when Au_{25} is incorporated in BSA. Finally, upon incorporation of Au_{25} nanoclusters into BSA, some structural reorganization, e.g. Au_{25} sphere-like to Au_{25} rod-like shape may occur.[28] However, again the 800 nm optical absorption shoulder is no more observed for rod-like Au_{25}. Also we found that "rod-like" shape clusters are not stable. Notice that "rod-like" shape Au_{25} nanoclusters were found with totally different staple ligands and counterions (e.g. $[Au_{25}(PPh3)_{10}(SC_2H_5)_5Cl_2]^{2+}$).[29] In the same vein, a topological isomer of the $Au_{25}(SR)_{18}$ nanocluster was proposed by Aikens and Hakkinen.[30] However, our calculations at the DFT level show that this isomer with pMBA ligands is considerably less stable than the known crystal structure for Au_{25}. In addition, the topological isomers present very different absorption spectra than the one reported for known crystal structure for Au_{25}.[29]-[30]

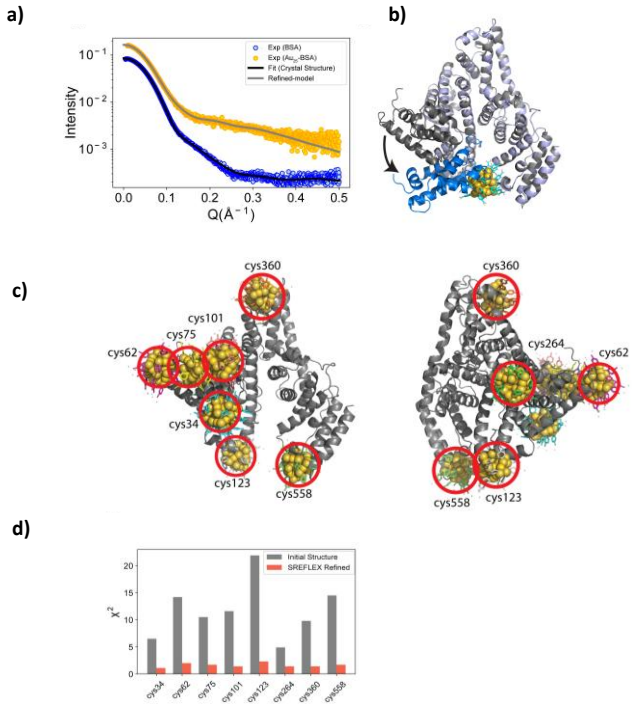


Figure 3 : a) The experimental SAXS profiles of BSA (blue) overlaid with the theoretical SAXS profile of BSA monomer calculated using Crysol (black) and the SAXS profile of Au25-BSA (orange) overlaid with the theoretical SAXS profile of the SREFLEX refined model with Au25 bound to Cys34. b) The SREFLEX refined model of the Au25-BSA (light blue) superimposed on the crystal structure of BSA. The position of the part that was allowed to be moved by SREFLEX is shown in darker shades of the same colors in both structures. c) Two views of the BSA conjugated to Au25 at various cysteines, tested to determine the agreement with the SAXS data. d) The χ2 values between the theoretical SAXS profile of BSA conjugated to Au25 at different cysteines calculated directly from the structure using Crysol (gray bars) or after refinement using SREFLEX (red bars).

Secondary structural changes in the BSA upon Au_{25} NC incorporation were measured by circular dichroism (CD) spectroscopy, which is shown in Figure S5. The CD spectra of the BSA and Au_{25}-BSA are very similar, suggesting that the Au_{25}-BSA retained the α-helicity to a high degree. This observation also confirms the low perturbation of the protein secondary structure content. These results are in stark contrast to the results of Xie's classical method, which was performed under alkaline conditions, and they show the advantage of the synthetic methodology developed here.[13] FT-

IR spectra of Au_{25}p-MBA_{18}, Au_{25}-BSA and BSA are shown in Figure S6. Of note FT-IR spectra of both Au_{25}-BSA and BSA are very similar showing that Au_{25} do not affect to much the overall environment of the vibrational bonds involved in the spectra (mainly amine bands I and II).

Small-angle X-ray scattering (SAXS) is a widely used technique for the structural and dynamic characterization of biomolecules in aqueous solutions.[31] To obtain the scattering profiles of BSA and the Au_{25}-BSA complex, inline size-exclusion chromatography coupled to SAXS (SEC-SAXS) was used, as it enables the separation of the major peak corresponding to the BSA monomer from those of the BSA oligomers (Fig. S7). Consistent with its larger molecular weight, Au_{25}-BSA eluted earlier than native BSA. SEC-SAXS frames corresponding to the monomer were averaged using standard procedures for subsequent structural analyses. The SAXS profiles of BSA and Au_{25}-BSA present different features along the momentum transfer range measured, indicating that the presence of the Au_{25} NC strongly modifies the scattering properties of the protein (Fig. 3). As expected, Au_{25}-BSA presents a slightly larger radius of gyration, R_g, than free BSA, 28.16 ± 0.05 Å and 27.95 ± 0.02 Å and, respectively. We have also performed SAXS experiments on a Au_{25}pMBA_{18} sample. Although the measured scattering profile exhibited aggregation features at low q-values, a Rg value of 6.5 +/- 0.1 Å could be derived. When computing the pairwise distance distribution, p(r), we found that the unmodified BSA had a D_{max} of 82.1 Å, similar to the value identified in earlier studies,[32] and a symmetric p(r) profile typical of globular proteins. In contrast, Au_{25}-BSA had a significantly larger D_{max} of 90.85 Å and had a shoulder at small distances, indicating the presence of additional scattering centers in the protein.

Next, the capacity of the crystallographic structure of BSA (PDB entry 3v03) was evaluated to describe both SAXS curves shown in Fig. 3a. While the structure was in excellent agreement with the BSA profile (χ^2 = 2.2) (Fig. 3a), unsurprisingly, it was unable to describe the curve measured for Au_{25}-BSA (χ^2 = 24.6). To achieve a better fit between the experimental data and the theoretical structure of the Au_{25}-BSA, we modeled the Au_{25} NC (see Computational for Au_{25} NC details in the SI) on the surface of the BSA. We selected Cys_{34} for this model, as it is the only free cysteine in the protein, and we placed its side chain in the position of one of the pMBA molecules of the external protective shell of the Au NC (Fig. 3b). Although the incorporation of the Au_{25} NC into the BSA structure improved the agreement with the experimental Au_{25}-BSA SAXS curve (χ^2 = 6.55), systematic deviations throughout the momentum transfer range were still observed. A closer inspection of the BSA structure showed a region of the protein (residues 55-119), consisting of a long unstructured loop (residues 105-119), that could be structurally impacted in the presence of the NC. To test this hypothesis, we performed a normal mode SAXS refinement of the Au_{25}-BSA structure using the program SREFLEX,[33] allowing movement in this region while maintaining the rest of the protein and keeping the NC fixed in place (Fig. 3b).

To show the selectivity of NC binding, we generated seven different structures with the Au_{25} NC attached to other cysteines of the BSA (Fig. 3c). Note that these cysteines are engaged in disulfide bonds in the native structure. For six of the Au_{25}-BSA complexes, the resulting structures displayed worse χ^2 values than the model built using Cys_{34} as the anchoring point (Fig. 3d). Even after normal mode refinement, all the resulting structures provide worse agreement with the experimental data than the Cys_{34}-anchored structure. In short, the SAXS analyses strongly indicate that the Au_{25} NC selectively binds to free Cys_{34} and that this binding induces structural perturbations to accommodate the metallic cluster.

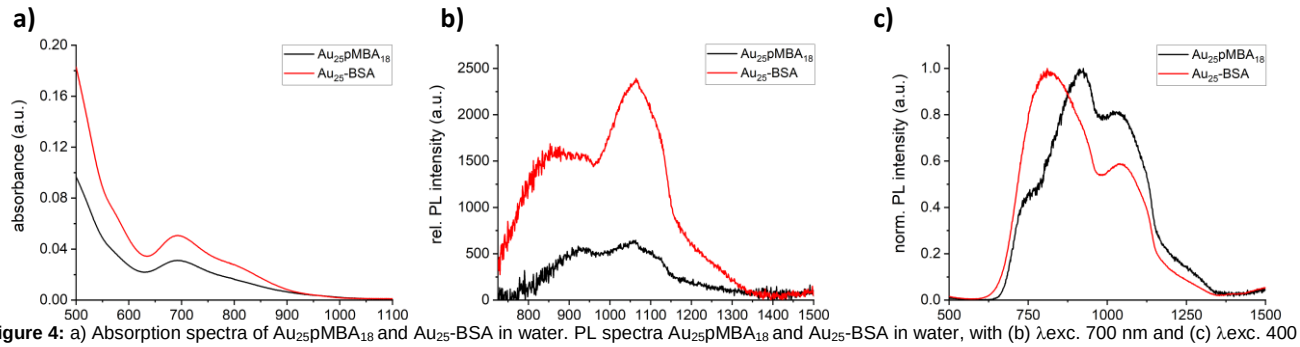


Figure 4: a) Absorption spectra of Au_{25}pMBA_{18} and Au_{25}-BSA in water. PL spectra Au_{25}pMBA_{18} and Au_{25}-BSA in water, with (b) λexc. 700 nm and (c) λexc. 400 nm.

Optical properties of the Au_{25}pMBA_{18} and Au_{25}-BSA NCs. The attachment of Au_{25} to BSA leads to a significant enhancement of the PL signal (upon excitation at 700 nm) at both 850 nm and 1050 nm, as seen in Figure 4b, with a 4.7-fold increase in QY (see Table S1). A similar trend is observed for excitation at 400 nm (see Fig. 4c). To confirm that this effect is not only due to simple physisorption of Au_{25} NCs onto BSA, steady-state and time-resolved PL measurements (Figure S8) of Au_{25}pMBA_{18} and Au_{25}-BSA were performed in water, and Au_{25}pMBA_{18} was analyzed in the presence of a high BSA concentration (50 mg/mL). Although the addition of BSA resulted in a PL intensity enhancement, the overall effect was much lower than that of direct incorporation. Better insight into the influence of BSA on the fluorescence kinetics of Au NCs can be obtained by time-resolved measurements. The addition of BSA to the Au NC solution resulted in an increase in the average amplitude weighted lifetime from 72.1 ns to 396.3 ns. However, the Au_{25}-BSA complex possessed a PL lifetime of 936.1 ns, which indicates that the local environment of the Au_{25} NCs in Au_{25}-BSA is more rigid than that of free Au_{25}pMBA_{18} dispersed in water or in the presence of unbound protein. Therefore, the tight entrapment of Au_{25} in the protein scaffold of Au_{25}-BSA is prone to multiple energy transfers associated with intersystem crossings (vide infra).

The absence of any changes in the PL intensity and lifetime of the Au_{25}-BSA complex when added to a concentrated BSA solution is additional evidence for the successful incorporation of the cluster in the BSA protein and thus protection from its environmental surroundings (Figure S9 and Table S2), indicating the presence of a strong protective shell around the Au_{25} in this labeled protein. To note is that BSA-Au NCs could keep their photophysical and chemical

properties when kept in solution in the fridge for more than 2 months but could be also lyophilized for a long-term storage.

In summary, by attaching a single Au_{25} NC to BSA through ligand exchange between protecting pMBA ligands and natural sulfur-containing BSA cysteine residues, we managed to tailor the NIR-II signal while keeping the structure of Au_{25} intact. Interestingly, the ratio between the relative intensity at 920 nm and 1050 nm strongly depends on the excitation wavelength (compare $\lambda_{exc.}$ = 400 nm and $\lambda_{exc.}$ = 700 nm, see Fig. 4 and Table S3). The ratio is also dependent on the nature of the ligands protecting the Au_{25} (for a comparison of $Au_{25}pMB_{A18}$ and Au_{25}-BSA, see Table S3). To better understand the PL properties of the Au_{25} nanoclusters that attach to BSA more favourably via cysteine residues, which was suggested by the SAXS/MS results, we synthesized mixed liganded nanoclusters, $Au_{25}pMBA_{(18-x)}Cys_x$ with x= 2, 5, 18, through ligand exchange. Optical measurements and density functional theory allowed us to determine the key role of the metallic-ligand interface in the photophysical pathways.

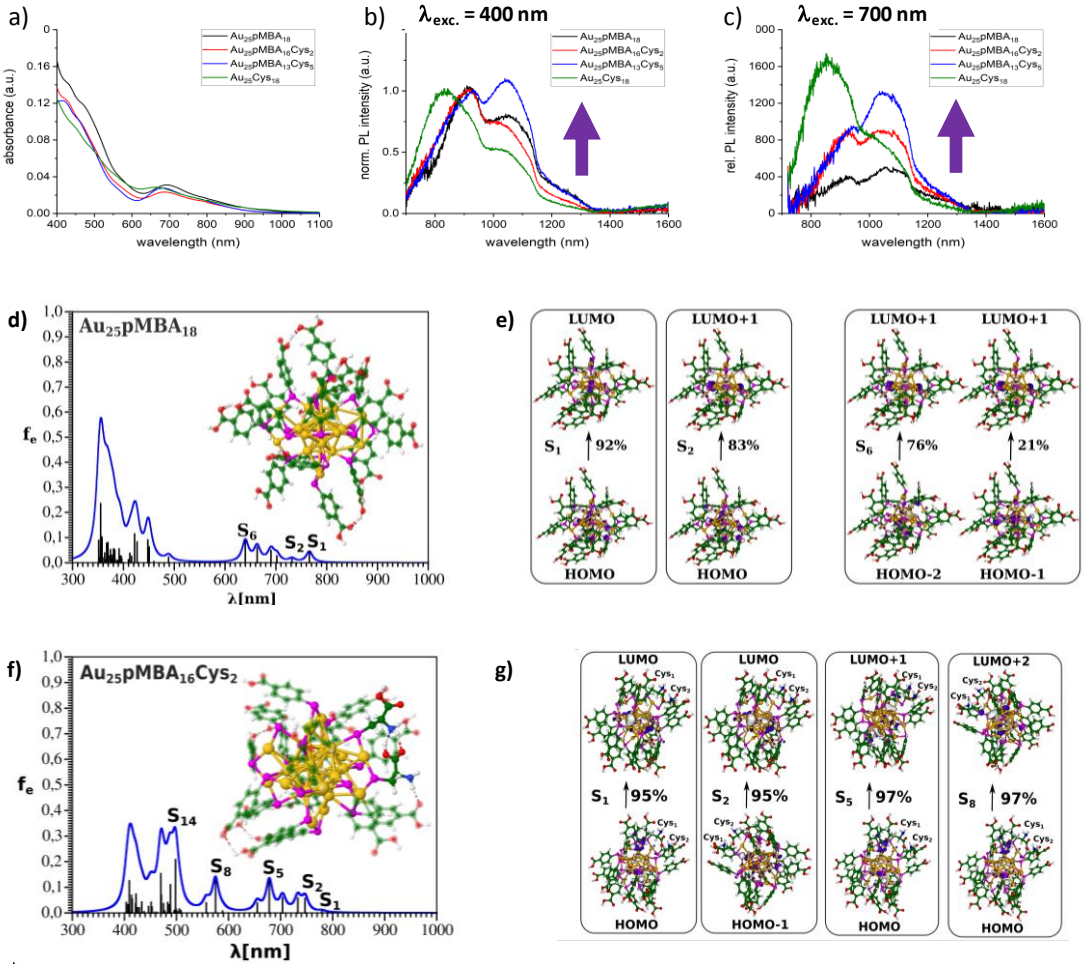


Figure 5: (a) Absorbance spectra and (b,c) normalized PL spectra of $Au_{25}pMBA_{(18-x)}Cys_x$ solutions dispersed in water. d) and e) TD-DFT results on $Au_{25}pMBA_{18}$: absorption spectrum and molecular orbitals involved in the first excited state transitions, showing involvement of the gold core and contributions from Au-S, Au or S. f) and g) TD-DFT results on the $Au_{25}pMBA_{16}Cys_2$ absorption spectrum and molecular orbitals involved in the first excited state transitions, showing the involvement of the gold core and contributions from Au-S, Au or S. Of note, DFT calculations with structures with two Cys on adjacent staples but not on the same staple. is found to be higher in energy than the structure with the Cysteines exchanged on the same staple (see fig. S12).

Insight into the relationship between the structure and optical properties and the origin of the NIR-II emission. The PL of metal nanoclusters originates from a subtle interplay between excitations arising within the metal core and from charge transfer between the metal core and surface ligands.[34] However, the detailed PL mechanism of gold nanoclusters is still under debate.[35] The high stability and detailed structure determination of $Au_{25}(SR)_{18}$ (gold nanoclusters protected by SR thiolate ligands) enabled extensive investigation of the relationship between the structure and optical properties; in particular, it enabled the study of its PL properties. Upon visible excitation, both red (700−800 nm) and near-infrared emissions (approximately and above 1000 nm) have been observed in $Au_{25}(SR)_{18}$ by different groups.[36] On the basis of time-resolved emission and nanosecond transient absorption spectroscopy analyses, Meng Zhou and Yongbo Song proposed a simplified model,[36c] where visible and near-infrared emissions have different lifetimes and arise from the core−interface charge transfer state and the Au_{13} core state, respectively.

When Au_{25} is incorporated into BSA, at least one ligand exchange with the protein occurs via a cysteine residue, which significantly modifies the PL profile (Fig. 4). To reveal the key role of the metallic-ligand interface in the photophysical pathways of BSA-Au NCs, we produced $Au_{25}pMBA_{(18-x)}Cys_x$ NCs with x=0, 2, 5, and 18 by ligand exchange (between pMBA and cysteine) from the $Au_{25}pMBA_{18}$ precursor nanocluster. These NCs were fully characterized by ESI-MS (see Fig. S10). $Au_{25}pMBA_{(18-x)}Cys_x$ with x=0, <2>, <5> and 18 presents the typical absorption features of Au_{25} NCs with the characteristic band centered at 690 nm, as well as a broad shoulder at ~800 nm (Figure 5a).[37] The PL profile of these Au_{25} NCs dispersed in water exhibits two main broad bands at 800-950 nm and 1050-1250 nm (Fig. 5b and c). When the number of Cys molecules on the Au NC surface increased from 2 to 5, an increase in the PL and at 1050 nm was observed (see Fig. 5b and c). To compare the evolution of the two main NIR-II emission bands, we determined the PL ratio of the peak at 1050 nm to that at 920 nm to determine if there is a correlation between the presence of the co-ligand and the PL enhancement at 1050 nm (Table S3). The results indicated a more pronounced effect when 700 nm was used as the excitation wavelength than when 400 nm was used, indicating that the 1050 nm emission probably involves photophysical relaxation pathways taking place within the metal core as it was nicely demonstrated by Zhou and Song based on time-resolved emission and nanosecond transient absorption spectroscopy analyses.[36c] However, with the protein environment, we cannot exclude that the band at 1050 nm might also originate from the surface with solvatochromism, rigidity and the presence of the long components of the fluorescent lifetime sensitive to the environments. Indeed, with an excitation wavelength of 700 nm, the lowest energy excited states (S_1, S_2) are mainly involved in photoexcitation, as confirmed by the time-dependent density functional theory (TD-DFT) linear absorption spectrum (Fig. 5d and 5f, and see computational details in SI). Low-lying states in the NIR are key to obtaining large two-photon absorption cross sections (due to double resonance effects), which would make them ideal labels for multiphoton excited luminescence (see Fig. S11). The lowest excited states in the absorption spectrum mainly belong to the “core” in nature, primarily arising from transitions from the occupied P orbitals into the first and second sets of D orbitals (see Fig. 5e and Table S4). For low-lying excited states, some contributions of the ligands to the transitions are more readily observed in $Au_{25}pMBA_{16}Cys_2$ than in $Au_{25}pMBA_{18}$ (Table S4). Under 400 nm excitation, the nature of excited states is both “interface-like” and “core-like”.[38] The characteristic of such excited states is mainly “interface-like” for which the contribution from the Au-S interface in orbitals is more pronounced, particularly in the cysteine-containing Au NCs (Table S4). Although pMBA and cysteine are rich electron donors, cysteine is more flexible due to the $C_{\square}$-$C_{\square}$ bond and is better able to interact with the surface of the gold core than pMBA, as its carboxylic group points outward toward the surface of the gold core. Such electron-rich donor groups may contribute to the “interface-like” excited states and thus may increase the contribution of the 850 nm band.

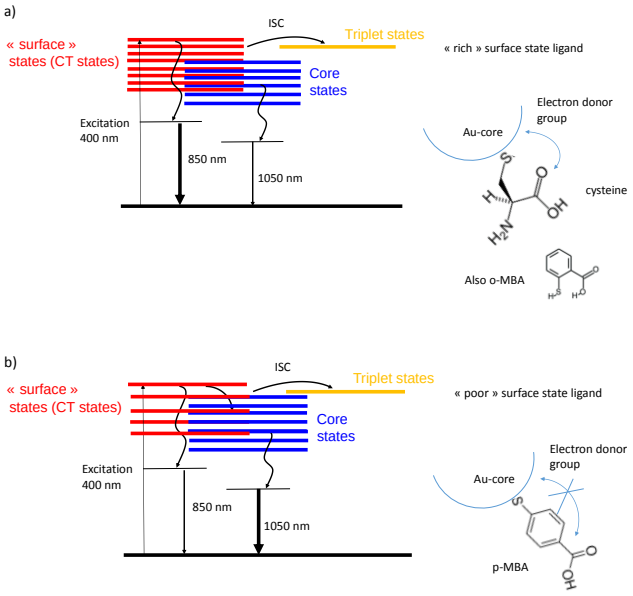


Figure 6: Proposed mechanism of emissions in Au_{25} nanoclusters with different surface ligands.

This phenomenon is particularly true for $Au_{25}Cys_{18}$, which mainly displays a strong emission at 850 nm. On the basis of these experimental and theoretical results, we propose the following mechanism to explain the relative contribution of

emission bands (at 850 and 1050 nm) of the Au_{25}-BSA conjugates (Figure 6): first, the local environment of Au_{25} NCs attached to BSA is more rigid than free $Au_{25}pMBA_{18}$ and prone to multiple energy transfers associated with intersystem crossing (reinforced ISC), which could explain the overall enhancement in PL emission and the longer PL lifetimes. Second, the nature of ligands, and in particular their capability to interact through electron-rich donor groups with the surface of the Au core, may increase the number of surface states involved in excitation (specifically at 400 nm).

Conclusion

Here, we present a simple route to attach individual Au_{25} NCs to a BSA protein via a cysteine residue. mass spectrometry (both MALDI-MS and ESI-MS) and SAXS and molecular modeling provide a clear localization of Au_{25} within the protein (Cys_{34}). The change in the local microenvironment of the Au NCs incorporated into the BSA boosts the NIR-II signal but preserves the structure of the Au_{25}. Rigidification of the surface molecules within the BSA protein reinforces the intersystem crossing pathway involved in photoluminescence. Cysteine ligands exchanged during the attachment of Au_{25} to BSA allow for an increased contribution of core−interface charge transfer states. Both effects induce enhancement and shift the photoluminescence signal. In addition to the importance of keeping the structure of Au NCs unchanged within the protein, which enables us to decipher the structure-property relationships, it is of interest to use 700 nm excitation for in vivo optical imaging and photoactivation, both in the linear and nonlinear optical regimes. This study paves the way to designing new photoemitters with tunable NIR-I/NIR-II emission via visible or NIR excitation. Finally, engineering mutations in proteins with cysteines will allow for more selective control of the position of atomically precise metal (Au, Ag, Pt, Cu…) NCs in proteins and of the number of ligands exchanged, opening new routes for extending their applications in diagnostic and therapeutic applications.[39]

Acknowledgements

This research was partly supported by the project STIM-REI, Contract Number: KK.01.1.1.01.0003, funded by the European Union through the European Regional Development Fund – the Operational Programme Competitiveness and Cohesion 2014–2020 (KK.01.1.1.01). VBK, MPB and HF acknowledge computational facilities of the HPC computer within the STIM-REI project, Doctoral study of Biophysics at University of Split as well as Prof. Miroslav Radman at MedILS and Split-Dalmatia County for support. This work was supported by the Labex EpiGenMed, an «Investissements d'avenir» program (ANR-10-LABX-12-01). The CBS is a member of France-BioImaging (FBI) and the French Infrastructure for Integrated Structural Biology (FRISBI), 2 national infrastructures supported by the French National Research Agency (ANR-10-INBS-04-01 and ANR-10-INBS-05, respectively). We thank the synchrotron facility SOLEIL (St. Aubin) for allocating regular beam time (20201085) and its dedicated staff for technical help with the beamline SWING. XLG would like to acknowledge Plan Cancer (C18038CS) and ANR SIREN (ANR-20CE09-0039-01) for their financial support. The authors would like to thank Céline Brunon, Julien Almaric and Esther Jarrossay from Science et Surface (www.science-et-surface.fr) for FTIR spectra.

Keywords: nanoclusters • proteins • luminescence • gold • SWIR/NIR-II

[1] a) N. Goswami, Z. Luo, X. Yuan, D. T. Leong, J. Xie, *Materials Horizons* **2017**, *4*, 817-831; b) X. Qu, Y. Li, L. Li, Y. Wang, J. Liang, J. Liang, *Journal of Nanomaterials* **2015**, *2015*, 23; c) L. Zhang, E. Wang, *Nano Today* **2014**, *9*, 132-157; d) E. Porret, X. Le Guével, J.-L. Coll, *Journal of Materials Chemistry B* **2020**, *8*, 2216-2232; e) Y. Zheng, J. Wu, H. Jiang, X. Wang, *Coordination Chemistry Reviews* **2021**, *431*, 213689.

[2] A. D. Kurdekar, L. A. A. Chunduri, C. S. Manohar, M. K. Haleyurgirisetty, I. K. Hewlett, K. Venkataramaniah, *Science Advances* **2018**, *4*, eaar6280.

[3] a) X. Kang, M. Zhu, *Chemical Society Reviews* **2019**, *48*, 2422-2457; b) S. Zhu, X. Wang, Y. Cong, L. Li, *ACS Omega* **2020**, *5*, 22702-22707.

[4] a) K. Pyo, V. D. Thanthirige, K. Kwak, P. Pandurangan, G. Ramakrishna, D. Lee, *Journal of the American Chemical Society* **2015**, *137*, 8244-8250; b) F. Bertorelle, C. Moulin, A. Soleilhac, C. Comby-Zerbino, P. Dugourd, I. Russier-Antoine, P.-F. Brevet, R. Antoine, *ChemPhysChem* **2018**, *19*, 165-168; c) X. L. Guevel, O. Tagit, C. E. Rodríguez, V. Trouillet, M. Pernia Leal, N. Hildebrandt, *Nanoscale* **2014**, *6*, 8091-8099.

[5] Y. Chen, D. M. Montana, H. Wei, J. M. Cordero, M. Schneider, X. Le Guével, O. Chen, O. T. Bruns, M. G. Bawendi, *Nano Letters* **2017**, *17*, 6330-6334.

[6] M. Perić, Ž. Sanader Maršić, I. Russier-Antoine, H. Fakhouri, F. Bertorelle, P.-F. Brevet, X. le Guével, R. Antoine, V. Bonačić-Koutecký, *Physical Chemistry Chemical Physics* **2019**, *21*, 23916-23921.

[7] B. Zhang, J. Chen, Y. Cao, O. J. H. Chai, J. Xie, *Small*, *n/a*, 2004381.

[8] S. E. Crawford, M. J. Hartmann, J. E. Millstone, *Accounts of Chemical Research* **2019**, *52*, 695-703.

[9] a) S. E. Crawford, C. M. Andolina, A. M. Smith, L. E. Marbella, K. A. Johnston, P. J. Straney, M. J. Hartmann, J. E. Millstone, *Journal of the American Chemical Society* **2015**, *137*, 14423-14429; b) C. M. Andolina, A. C. Dewar, A. M. Smith, L. E. Marbella, M. J. Hartmann, J. E. Millstone, *Journal of the American Chemical Society* **2013**, *135*, 5266-5269.

[10] B. Musnier, K. D. Wegner, C. Comby-Zerbino, V. Trouillet, M. Jourdan, I. Häusler, R. Antoine, J.-L. Coll, U. Resch-Genger, X. Le Guével, *Nanoscale* **2019**, *11*, 12092-12096.

[11] Z. Yu, B. Musnier, K. D. Wegner, M. Henry, B. Chovelon, A. Desroches-Castan, A. Fertin, U. Resch-Genger, S. Bailly, J.-L. Coll, Y. Usson, V. Josserand, X. Le Guével, *ACS Nano* **2020**, *14*, 4973-4981.

[12] I. Zare, D. M. Chevrier, A. Cifuentes-Rius, N. Moradi, Y. Xianyu, S. Ghosh, L. Trapiella-Alfonso, Y. Tian, A. Shourangiz-Haghighi, S. Mukherjee, K. Fan, M. R. Hamblin, *Materials Today* **2021**.

[13] J. Xie, Y. Zheng, J. Y. Ying, *Journal of the American Chemical Society* **2009**, *131*, 888-889.

[14] a) L. Shang, S. Dong, G. U. Nienhaus, *Nano Today* **2011**, *6*, 401-418; b) L. Shang, G. U. Nienhaus, *Biophysical Reviews* **2012**, *4*, 313-322; c) L. Shang, J. Xu, G. U. Nienhaus, *Nano Today* **2019**, *28*, 100767.

[15] a) C.-L. Liu, H.-T. Wu, Y.-H. Hsiao, C.-W. Lai, C.-W. Shih, Y.-K. Peng, K.-C. Tang, H.-W. Chang, Y.-C. Chien, J.-K. Hsiao, J.-T. Cheng, P.-T. Chou, *Angew. Chem. Int. Ed.* **2011**, *50*, 7056-7060; b) Q.-Q. Zhuang, H.-H. Deng, S.-B. He, H.-P. Peng, Z. Lin, X.-H. Xia, W. Chen, *ACS Applied Materials & Interfaces* **2019**, *11*, 31729-31734; c) Q.-Q. Zhuang, R.-T. Chen, Y.-J. Zheng, K.-Y. Huang, H.-P. Peng, Z. Lin, X.-H. Xia, W. Chen, H.-H. Deng, *Biosensors and Bioelectronics* **2021**, *177*, 112977.

[16] a) A. Soleilhac, F. Bertorelle, R. Antoine, *Spectrochimica Acta Part A: Molecular and Biomolecular Spectroscopy* **2018**, *193*, 283-288; b) A. Baksi, A. Mitra, J. S. Mohanty, H. Lee, G. De, T. Pradeep, *The Journal of Physical Chemistry C* **2015**, *119*, 2148-2157; c) D. Ghosh, A. Baksi, S. K. Mudedla, A. Nag, M. A. Ganayee, V. Subramanian, T. Pradeep, *The Journal of Physical Chemistry C* **2017**, *121*, 13335-13344; d) K. Chaudhari, P. L. Xavier, T. Pradeep, *ACS Nano* **2011**, *5*, 8816-8827; e) M. Kluz, H. Nieznańska, R. Dec, I. Dzięcielewski, B. Nižyński, G. Ścibisz, W. Puławski, G. Staszczak, E. Klein, J. Smalc-Koziorowska, W. Dzwolak, *PLOS ONE* **2019**, *14*, e0218975.

[17] a) D. M. Chevrier, V. D. Thanthirige, Z. Luo, S. Driscoll, P. Cho, M. A. MacDonald, Q. Yao, R. Guda, J. Xie, E. R. Johnson, A. Chatt, N. Zheng, P. Zhang, *Chemical Science* **2018**, *9*, 2782-2790; b) H. A. Kindi, A. Mohamed, S. Kajimoto, N. Zhanpeisov, H. Horino, Y. Shibata, I. I. Rzeznicka, H. Fukumura, *Journal of Photochemistry and Photobiology A: Chemistry* **2018**, *357*, 168-174.

[18] Y. Wang, T. Bürgi, *Nanoscale Advances* **2021**, *3*, 2710-2727.

[19] a) G. F. Combes, H. Fakhouri, C. Moulin, M. Girod, F. Bertorelle, S. Basu, R. Ladouce, M. P. Bakulić, Ž. S. Maršić, I. Russier-Antoine, P.-F. Brevet, P. Dugourd, A. Krisko, K. Trajković, M. Radman, V. Bonačić-Koutecký, R. Antoine, *Communications Chemistry* **2021**, *4*, 69; b) G. F. Combes, A.-M. Vučković, M. Perić Bakulić, R. Antoine, V. Bonačić-Koutecky, K. Trajković, *Cancers* **2021**, *13*, 4206.

[1] a) N. Goswami, Z. Luo, X. Yuan, D. T. Leong, J. Xie, *Materials Horizons* **2017**, *4*, 817-831; b) X. Qu, Y. Li, L. Li, Y. Wang, J. Liang, J. Liang, *Journal of Nanomaterials* **2015**, *2015*, 23; c) L. Zhang, E. Wang, *Nano Today* **2014**, *9*, 132-157; d) E. Porret, X. Le Guével, J.-L. Coll, *Journal of Materials Chemistry B* **2020**, *8*, 2216-2232; e) Y. Zheng, J. Wu, H. Jiang, X. Wang, *Coordination Chemistry Reviews* **2021**, *431*, 213689.

[2] A. D. Kurdekar, L. A. A. Chunduri, C. S. Manohar, M. K. Haleyurgirisetty, I. K. Hewlett, K. Venkataramaniah, *Science Advances* **2018**, *4*, eaar6280.

[3] a) X. Kang, M. Zhu, *Chemical Society Reviews* **2019**, *48*, 2422-2457; b) S. Zhu, X. Wang, Y. Cong, L. Li, *ACS Omega* **2020**, *5*, 22702-22707.

[4] a) K. Pyo, V. D. Thanthirige, K. Kwak, P. Pandurangan, G. Ramakrishna, D. Lee, *Journal of the American Chemical Society* **2015**, *137*, 8244-8250; b) F. Bertorelle, C. Moulin, A. Soleilhac, C. Comby-Zerbino, P. Dugourd, I. Russier-Antoine, P.-F. Brevet, R. Antoine, *ChemPhysChem* **2018**, *19*, 165-168; c) X. L. Guevel, O. Tagit, C. E. Rodríguez, V. Trouillet, M. Pernia Leal, N. Hildebrandt, *Nanoscale* **2014**, *6*, 8091-8099.

[5] Y. Chen, D. M. Montana, H. Wei, J. M. Cordero, M. Schneider, X. Le Guével, O. Chen, O. T. Bruns, M. G. Bawendi, *Nano Letters* **2017**, *17*, 6330-6334.

[6] M. Perić, Ž. Sanader Maršić, I. Russier-Antoine, H. Fakhouri, F. Bertorelle, P.-F. Brevet, X. le Guével, R. Antoine, V. Bonačić-Koutecký, *Physical Chemistry Chemical Physics* **2019**, *21*, 23916-23921.

[7] B. Zhang, J. Chen, Y. Cao, O. J. H. Chai, J. Xie, *Small*, *n/a*, 2004381.

[8] S. E. Crawford, M. J. Hartmann, J. E. Millstone, *Accounts of Chemical Research* **2019**, *52*, 695-703.

[9] a) S. E. Crawford, C. M. Andolina, A. M. Smith, L. E. Marbella, K. A. Johnston, P. J. Straney, M. J. Hartmann, J. E. Millstone, *Journal of the American Chemical Society* **2015**, *137*, 14423-14429; b) C. M. Andolina, A. C. Dewar, A. M. Smith, L. E. Marbella, M. J. Hartmann, J. E. Millstone, *Journal of the American Chemical Society* **2013**, *135*, 5266-5269.

[10] B. Musnier, K. D. Wegner, C. Comby-Zerbino, V. Trouillet, M. Jourdan, I. Häusler, R. Antoine, J.-L. Coll, U. Resch-Genger, X. Le Guével, *Nanoscale* **2019**, *11*, 12092-12096.

[11] Z. Yu, B. Musnier, K. D. Wegner, M. Henry, B. Chovelon, A. Desroches-Castan, A. Fertin, U. Resch-Genger, S. Bailly, J.-L. Coll, Y. Usson, V. Josserand, X. Le Guével, *ACS Nano* **2020**, *14*, 4973-4981.

[12] I. Zare, D. M. Chevrier, A. Cifuentes-Rius, N. Moradi, Y. Xianyu, S. Ghosh, L. Trapiella-Alfonso, Y. Tian, A. Shourangiz-Haghighi, S. Mukherjee, K. Fan, M. R. Hamblin, *Materials Today* **2021**.

[13] J. Xie, Y. Zheng, J. Y. Ying, *Journal of the American Chemical Society* **2009**, *131*, 888-889.

[14] a) L. Shang, S. Dong, G. U. Nienhaus, *Nano Today* **2011**, *6*, 401-418; b) L. Shang, G. U. Nienhaus, *Biophysical Reviews* **2012**, *4*, 313-322; c) L. Shang, J. Xu, G. U. Nienhaus, *Nano Today* **2019**, *28*, 100767.

[15] a) C.-L. Liu, H.-T. Wu, Y.-H. Hsiao, C.-W. Lai, C.-W. Shih, Y.-K. Peng, K.-C. Tang, H.-W. Chang, Y.-C. Chien, J.-K. Hsiao, J.-T. Cheng, P.-T. Chou, *Angew. Chem. Int. Ed.* **2011**, *50*, 7056-7060; b) Q.-Q. Zhuang, H.-H. Deng, S.-B. He, H.-P. Peng, Z. Lin, X.-H. Xia, W. Chen, *ACS Applied Materials & Interfaces* **2019**, *11*, 31729-31734; c) Q.-Q. Zhuang, R.-T. Chen, Y.-J. Zheng, K.-Y. Huang, H.-P. Peng, Z. Lin, X.-H. Xia, W. Chen, H.-H. Deng, *Biosensors and Bioelectronics* **2021**, *177*, 112977.

[16] a) A. Soleilhac, F. Bertorelle, R. Antoine, *Spectrochimica Acta Part A: Molecular and Biomolecular Spectroscopy* **2018**, *193*, 283-288; b) A. Baksi, A. Mitra, J. S. Mohanty, H. Lee, G. De, T. Pradeep, *The Journal of Physical Chemistry C* **2015**, *119*, 2148-2157; c) D. Ghosh, A. Baksi, S. K. Mudedla, A. Nag, M. A. Ganayee, V. Subramanian, T. Pradeep, *The Journal of Physical Chemistry C* **2017**, *121*, 13335-13344; d) K. Chaudhari, P. L. Xavier, T. Pradeep, *ACS Nano* **2011**, *5*, 8816-8827; e) M. Kluz, H. Nieznańska, R. Dec, I. Dzięcielewski, B. Nižyński, G. Ścibisz, W. Puławski, G. Staszczak, E. Klein, J. Smalc-Koziorowska, W. Dzwolak, *PLOS ONE* **2019**, *14*, e0218975.

[17] a) D. M. Chevrier, V. D. Thanthirige, Z. Luo, S. Driscoll, P. Cho, M. A. MacDonald, Q. Yao, R. Guda, J. Xie, E. R. Johnson, A. Chatt, N. Zheng, P. Zhang, *Chemical Science* **2018**, *9*, 2782-2790; b) H. A. Kindi, A. Mohamed, S. Kajimoto, N. Zhanpeisov, H. Horino, Y. Shibata, I. I. Rzeznicka, H. Fukumura, *Journal of Photochemistry and Photobiology A: Chemistry* **2018**, *357*, 168-174.

[18] Y. Wang, T. Bürgi, *Nanoscale Advances* **2021**, *3*, 2710-2727.

[19] a) G. F. Combes, H. Fakhouri, C. Moulin, M. Girod, F. Bertorelle, S. Basu, R. Ladouce, M. P. Bakulić, Ž. S. Maršić, I. Russier-Antoine, P.-F. Brevet, P. Dugourd, A. Krisko, K. Trajković, M. Radman, V. Bonačić-Koutecký, R. Antoine, *Communications Chemistry* **2021**, *4*, 69; b) G. F. Combes, A.-M. Vučković, M. Perić Bakulić, R. Antoine, V. Bonačić-Koutecky, K. Trajković, *Cancers* **2021**, *13*, 4206.

[20] F. Bertorelle, I. Russier-Antoine, C. Comby-Zerbino, F. Chirot, P. Dugourd, P.-F. Brevet, R. Antoine, *ACS Omega* **2018**, *3*, 15635-15642.

[21] a) Y. Yu, Z. Luo, Y. Yu, J. Y. Lee, J. Xie, *ACS Nano* **2012**, *6*, 7920-7927; b) C. Comby-Zerbino, F. Bertorelle, P. Dugourd, R. Antoine, F. Chirot, *The Journal of Physical Chemistry A* **2020**, *124*, 5840-5848.

[22] a) X. Kang, H. Chong, M. Zhu, *Nanoscale* **2018**, *10*, 10758-10834; b) M. Zhu, C. M. Aikens, F. J. Hollander, G. C. Schatz, R. Jin, *Journal of the American Chemical Society* **2008**, *130*, 5883-5885.

[23] R. Jin, *Nanoscale* **2015**, *7*, 1549-1565.

[24] M. Zhu, H. Qian, R. Jin, *The Journal of Physical Chemistry Letters* **2010**, *1*, 1003-1007.

[25] a) A. Das, T. Li, K. Nobusada, C. Zeng, N. L. Rosi, R. Jin, *Journal of the American Chemical Society* **2013**, *135*, 18264-18267; b) M. Waszkielewicz, J. Olesiak-Banska, C. Comby-Zerbino, F. Bertorelle, X. Dagany, A. K. Bansal, M. T. Sajjad, I. D. W. Samuel, Z. Sanader, M. Rozycka, M. Wojtas, K. Matczyszyn, V. Bonacic-Koutecky, R. Antoine, A. Ozyhar, M. Samoc, *Nanoscale* **2018**, *10*, 11335-11341.

[26] Y. Zhou, L. Liao, S. Zhuang, Y. Zhao, Z. Gan, W. Gu, J. Li, H. Deng, N. Xia, Z. Wu, *Angewandte Chemie International Edition* **2021**, *60*, 8668-8672.

[27] M. Zhu, W. T. Eckenhoff, T. Pintauer, R. Jin, *The Journal of Physical Chemistry C* **2008**, *112*, 14221-14224.

[28] X. Kang, M. Zhu, *Chemistry of Materials* **2019**, *31*, 9939-9969.

[29] Y. Shichibu, Y. Negishi, T. Watanabe, N. K. Chaki, H. Kawaguchi, T. Tsukuda, *The Journal of Physical Chemistry C* **2007**, *111*, 7845-7847.

[30] M. F. Matus, S. Malola, E. Kinder Bonilla, B. M. Barngrover, C. M. Aikens, H. Häkkinen, *Chemical Communications* **2020**, *56*, 8087-8090.

[31] a) M. H. Koch, P. Vachette, D. I. Svergun, *Quarterly reviews of biophysics* **2003**, *36*, 147-227; b) C. D. Putnam, M. Hammel, G. L. Hura, J. A. Tainer, *Quarterly reviews of biophysics* **2007**, *40*, 191-285; c) P. Bernadó, N. Shimizu, G. Zaccai, H. Kamikubo, M. Sugiyama, *Biochimica et Biophysica Acta (BBA) - General Subjects* **2018**, *1862*, 253-274.

[32] C. M. Jeffries, M. A. Graewert, C. E. Blanchet, D. B. Langley, A. E. Whitten, D. I. Svergun, *Nature protocols* **2016**, *11*, 2122-2153.

[33] A. Panjkovich, D. I. Svergun, *Physical Chemistry Chemical Physics* **2016**, *18*, 5707-5719.

[34] a) K. L. D. M. Weerawardene, C. M. Aikens, *Journal of the American Chemical Society* **2016**, *138*, 11202-11210; b) T. Q. Yang, B. Peng, B. Q. Shan, Y. X. Zong, J. G. Jiang, P. Wu, K. Zhang, *Nanomaterials (Basel, Switzerland)* **2020**, *10*.
[35] M. Zhou, R. Jin, *Annual Review of Physical Chemistry* **2021**, *72*, 121-142.
[36] a) S. Link, A. Beeby, S. FitzGerald, M. A. El-Sayed, T. G. Schaaff, R. L. Whetten, *The Journal of Physical Chemistry B* **2002**, *106*, 3410-3415; b) Z. Wu, R. Jin, *Nano Letters* **2010**, *10*, 2568-2573; c) M. Zhou, Y. Song, *The Journal of Physical Chemistry Letters* **2021**, *12*, 1514-1519.
[37] S. Zhao, N. Austin, M. Li, Y. Song, S. D. House, S. Bernhard, J. C. Yang, G. Mpourmpakis, R. Jin, *ACS Catalysis* **2018**, *8*, 4996-5001.
[38] C. M. Aikens, *Accounts of Chemical Research* **2018**, *51*, 3065-3073.
[39] a) G. Niu, L. Lang, D. O. Kiesewetter, Y. Ma, Z. Sun, N. Guo, J. Guo, C. Wu, X. Chen, *Journal of Nuclear Medicine* **2014**, *55*, 1150-1156; b) Y. Wang, L. Lang, P. Huang, Z. Wang, O. Jacobson, D. O. Kiesewetter, I. U. Ali, G. Teng, G. Niu, X. Chen, *Proceedings of the National Academy of Sciences* **2015**, *112*, 208-213; c) M. Benešová, C. A. Umbricht, R. Schibli, C. Müller, *Molecular Pharmaceutics* **2018**, *15*, 934-946.